JOURNAL OF AIRCRAFT
Vol. 48, No. 1, January–February 2011

Investigation on the Fatigue Life of an Al 8090 Helicopter Riveted T-Joint

F. Viganò,* A. Manes,† and M. Giglio‡
Politecnico di Milano, 20156 Milano, Italy

DOI: 10.2514/1.C031117

The rotorcraft airframe is a complex structure designed to satisfy different functions; since fatigue life is one of the most critical, it is important that the structural configuration be accurately studied. Because of the fact that the riveted joints play an important role in fatigue-life assessments, an accurate experimental and numerical safe-life fatigue evaluation was carried out. Specimen panels were exposed to different fatigue conditions in order to evaluate their endurance. A detailed finite element analysis was also carried out in order to obtain an accurate stress–strain field in the most stressed rivets, and the residual stress in the holes was obtained by a complete simulation of the riveting forming. Based on the fatigue data on Al 8090-T8 that is described in literature, a complete fatigue analysis was carried out that demonstrated the ability of the numerical model to predict failure correctly.

I. Introduction

ROTORCRAFT frames are designed to satisfy different functions; not only must they guarantee structural integrity and performance, but they must also comply with the requirements of lightness, low-cost maintenance, and easy failure detection. At present, the most common types of airframes are constructed using aluminum alloy panels joined together by metallic fasteners.

The structural reliability of riveted joints plays an important role not only insofar as the entire aircraft frame is concerned, but also in civil structures. Their main functions are connecting two or more structural components and transferring them among the loads. The presence of holes in the fastener and the geometrical discontinuity due to the assembly process make the joint one of the most stressed zones and thus critical in terms of the structural assessment of the component. For these reasons, the joint should be designed following in-depth analysis, taking into consideration all assessment procedures and choosing the most suitable one (damage tolerance, fail-safe, and safe-life methodology).

Moreover, it is important to bear in mind that helicopter frames are subjected to high-vibration load levels, and so fatigue life is a key factor insofar as structural integrity is concerned. The material used and its structural configuration (joints, stringers, T-cleats, etc.) must be carefully checked, in compliance with the fatigue-tolerance requirements imposed by civil regulations CS 29.571 [1]; this regulation calls for a complete fatigue-tolerance assessment that can be performed according to different design approaches: safe-life, flaw tolerance, etc.

In particular, conducting a fatigue analysis on joints is rather expensive and complex, due to several different factors that affect fatigue life: fastener stiffness, friction, residual stress, and assembly tolerance. To accurately predict the fatigue behavior of airframe joints, all these relevant factors should be considered in detail.

Furthermore, it is also likely that the traditional materials used until now will be replaced in the near future by more innovative ones. In fact, nowadays, Al-Li alloys are used as a replacement for some of the longest-serving commercial aluminum alloys, such as 2024 and 2114, for example. Compared with these materials, an 8090 alloy has a 10%-lower density and an 11%-higher elastic modulus. Its use is suitable in applications where damage tolerance behavior and lower density are critical aspects for engineering design. The main disadvantages of these alloys in structural assessment are the presence of reduced ductility and fracture toughness and accelerated fatigue-crack growth rates, especially in the case of small crack dimensions (short cracks). This behavior is potentially dangerous, especially in highly stressed regions such as the rivet holes, because it can induce fast crack nucleation and cause multisite damage.

Thus, the presence of holes, rivet contact, residual stress, and geometric discontinuity means that the riveted joints play a key role in assessing the structural integrity of a helicopter frame. Numerous papers analyzing the fatigue life of riveted joints in detail are available in literature. Urban [2] provided an extensive summary of these works and carried out static and fatigue tests on different riveted-joint configurations. Urban also showed that in order to obtain an accurate stress field with a view to establishing a good numerical/experimental correlation, a detailed finite element (FE) model is required. The experimental analysis outlined in [2] also showed the possible presence of fretting failure during the fatigue tests. That work focused on the view shared by scientists regarding the effects of rivet-head dimensions and secondary bending on the fatigue life of the joint.

The papers written by Fung and Smart [3,4] provided evidence of a numerical parametric and fatigue study of riveted lap joints. Using both numerical and experimental methods, they investigated the effect of the interference fit and the friction and clamping force on the fatigue life of the joint. Their results confirm the effects of these parameters on the fatigue behavior of riveted sheet joints.

The structural reliability of riveted joints is important not only in aircraft structures, but also in civil structures; Al-Emrani and Kliger [5] used an FE model and experimental tests to analyze a connection in a riveted railway bridge. These types of structures are subjected to high localized stress in the joint system; for this reason, the only way to predict this type of stress accurately is by means of detailed nonlinear FE models. Another key issue in the riveting process consists in the evaluation of residual stress and, consequently, the way in which this stress distribution is capable of affecting the fatigue strength of the joint. Deng and Hutchinson [6] carried out an extensive FE analysis on simplified solid-rivet geometry in order to obtain the residual and clamping stresses. Müller [7] carried out an extensive experimental investigation showing the influence of different parameters on fatigue life. One of the most significant parameters is the squeeze force; in fact, the fatigue life of joints increases when a large squeeze force is used. Similar experimental

Received 25 May 2010; revision received 5 October 2010; accepted for publication 3 November 2010. Copyright © 2010 by the American Institute of Aeronautics and Astronautics, Inc. All rights reserved. Copies of this paper may be made for personal or internal use, on condition that the copier pay the $10.00 per-copy fee to the Copyright Clearance Center, Inc., 222 Rosewood Drive, Danvers, MA 01923; include the code 0021-8669/11 and $10.00 in correspondence with the CCC.

*Temporary Researcher, Dipartimento di Meccanica, Via la Masa 1; fabio.vigano@mecc.polimi.it.

†Ph.D. Researcher, Assistant Professor, Dipartimento di Meccanica, Via la Masa 1; andrea.manes@polimi.it.

‡Associate Professor, Dipartimento di Meccanica, Via la Masa 1; marco.giglio@polimi.it.

results were also obtained on both aluminum lap joints and fiber/metal-laminate lap joints. De Rijck et al. [8] studied the influence of rivet-head dimensions on the fatigue life of joints. The results obtained demonstrated that the increase of the squeeze force induces a larger rivet-head diameter and, consequently, a longer fatigue life. This happens when the squeeze force reaches a limit value, over which an increase in the force does not result in an increase in fatigue life. Because of its strong influence, the deformed rivet-head dimension is also used as a parameter to evaluate the quality of the riveting process. In fact, in a study on the quality assessment of a riveting process, Wang et al. [9] implemented a control system in the rivet gun. This control, consisting of a governing air regulation and of a microprocessor, results in the achievement of a repeatable riveting procedure. The controller acts on the riveting force and, consequently, on the deformed rivet-head dimensions. New research on riveting technology is based on electromagnetic systems, because they are easy to control and offer a better rivet quality [10,11].

The residual stresses are another factor having a strong impact on the fatigue life of the joint. For this reason, it was essential to create an FE model that is capable of predicting them accurately. Matos et al. [12] carried out a numerical study on the residual stress field induced by the cold working process applied to the rivet hole and its effect on fatigue-life improvement. The effect of residual stress can also be negative and depends on riveting conditions (interference, clamping force, etc.). Szolwinski and Farris [13] analyzed the squeeze-force effect on residual stress using a nonlinear 2-D FE model. These residual stresses are generally compressive near the rivet/hole interface and are tensile at the internal points far from the hole area. Szolwinski and Farris pointed out that a fatigue crack can nucleate and propagate at this point. This is in contradiction to the claim that a fatigue crack starts at a hole/rivet interface. The crack-initiation points are recognizable following an in-depth analysis of the stress field after loading and unloading conditions.

Moreira et al. [14] analytically (weight function) and numerically evaluated the residual stress intensity factor (SIF) for different crack dimensions and for different value interferences. In any event, this interference is coupled with the squeeze force and, consequently, with the deformed rivet-head dimensions. Moreira et al. clearly showed that the residual SIF has a minimum value at a fixed distance from the rivet/hole interface. This distance increases with hole expansion, and the minimum residual stress decreases. By also considering the SIF curve of a loaded joint and its residual value, the maximum value of the total SIF could not be at the rivet/hole interface; consequently, fatigue-crack initiation cannot start at this point.

Nowadays, 3-D FE analysis of the rivets is mainly used to study the stress field after the riveting process. Bouchard et al. [15] and Porcaro et al. [16] simulated the 3-D riveting process numerically. Similarly, Kelly and Costello [17] approached a numerical analysis of the blind rivet process. Rans and Strznicky [18] numerically reproduced the application of a solid rivet in order to obtain induced residual stresses in jointed plates. The 3-D FE model of rivets can also be used to develop a simplified failure model for crashworthiness analysis [19].

The interference between the rivet and the hole is another important factor capable of influencing the fatigue life of a joint. In multifastener joints, the most important effect of manufacturing tolerance is on load redistribution among the rivets [20,21].

Simulation of the riveting process is intrinsically a highly nonlinear problem (high deformation, material behavior, geometry, and complex contacts) that requires the use of a dynamic explicit solver such as Abaqus/Explicit®, LS-Dyna®, and PAM-Crash® in order to be resolved numerically.

Based on the aforementioned research, the aim of this paper is a detailed fatigue-life evaluation of the riveted joint in the rear part of a helicopter fuselage. The fuselage consists of classical aerospace skin/stringer/rivet structures made, for the most part, of Al-Li alloy 8090-T81. The rear part of the fuselage is joined to the central one by means of a rear modular joint consisting of T-cleats connected to the stringer by solid rivets. The first part of the paper describes the experimental data related to full-scale panels. These data were obtained from two specimens employed during an in-depth experimental test campaign carried out on the panel specimens of a helicopter frame to investigate different types of rear joints. After this, a complete and detailed 3-D FE simulation was performed, considering both the riveting process and the fatigue-test load. The numerical analyses were carried out on three different FE models. The first is a global model of a panel complete with all features, the second is a detailed submodel of the joint, and the last is an even more detailed submodel of the most stressed riveted area in which the failure appears. These models were accurately validated using the data obtained from the experimental tests.

The numerical and experimental data are then analyzed together with the fatigue curve of the material, and the importance of an accurate full-process simulation for the fatigue assessment of the component is then highlighted.

II. General Description of the Component

Because of the fact that the rear fuselage of a helicopter is traditionally a modular metallic structure, this configuration gives the joints a critical structural function. According to the test requirements of the modular joint in the exact service configuration, a panel specimen of the full-scale real structure was built. In particular, the rear modular joint in the lower part of the panel was reproduced in full detail without any modifications from the real one. Figure 1 shows the specimen panel used in this paper. The fundamental dimensions of the panel are overall width 580 mm and overall height 550 mm. Considering the figure from the top, the panel consists of a reinforced

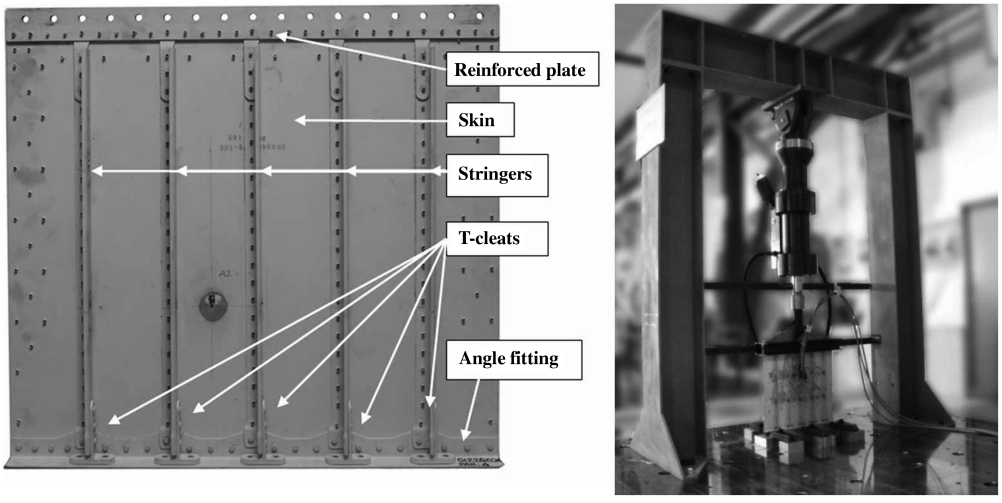

Fig. 1 Helicopter panel under analysis. The lower part of the panel is the real modular joint subjected to testing (left) and specimen installation (right).

Table 1 Applied loads and test results for each specimen panel

Specimen	Applied load, kN	Failure cycles
*P*2	2.16/21.6	830,530
*P*3	1.96/19.6	1,750,630

plate, which is useful for load application. Because of the fact that this is not critical for the fatigue life of the panel, this part was built in such a way as to allow not only the application of a load (as in the real structure), but also to avoid fatigue failure. Moving down toward the joint being tested, the specimen was designed in exactly the same way as a typical aeronautical structure, with a very thin skin and five shaped stringers joined together by rivets. At each side of the specimen panel, reinforcements were placed to avoid failure and to simulate the presence of the other panels found in the real configuration, which increase stiffness. These reinforcements are obviously not present in the real panel. As previously mentioned, the bottom of the panel is the critical part of the specimen. In this part, a piece of skin was folded in the angle fitting, joined by rivets to the main skin. The stringers were joined to the angle fitting by T-cleats. T-cleats are joined to the stringer by rivets and to the base part of the angle fitting by bolted joints. The bolted joint simulates the connection between the stringer and the ribs.

III. Experimental Tests

The main aim of the experimental tests was to analyze the fatigue-tolerance behavior of the structural joint. The specimens (described in the previous paragraph) were connected at the top to a hydraulic actuator by means of a stiff dedicated frame and were constrained at the bottom, near the modular joint, with two plates fixed to a working plane (Fig. 1). The upper connection consisted of a triangular plate, used to transfer the load from the actuator to the panel across the entire width and of two C-section beams to make the input load zone of the panels stiffer. To avoid rotation of the upper part, one C-section beam was connected by means of four rods to a fixed beam. Although the upper area was not subjected to testing, we felt that it would be useful to apply a load to the panel that reproduced the service load as closely as possible. The lower part of the specimen, simulating the rear modular joint structure, was fixed to a connection plate by means of a bolted connection with a calibrated tightening torque, thereby simulating real operating conditions. The connection plate was then fixed to the ground by another plate. The hydraulic actuator was attached to a rigid dedicated service structure. The value of the applied load was controlled by means of an internal load cell with a range of 100 kN. The tests were carried out in load control, using closed-loop instrumentation; an upper load limit of 105% of maximum applied force was set.

A sinusoidal load with a load ratio $R = 0.1$ was used to test the specimens. Table 1 shows the total applied force for each specimen and is the net weight of the dead load (self-weight, frame, and grip loads).

The first failure occurrence was used to evaluate the safe-life Wöhler data. Each fatigue test consisted of a safe-life phase, ranging from the beginning of the test to the first fatigue crack. The main output was the number of cycles of visible crack nucleation. The fatigue crack appeared on a T-cleat in the rivet connection with the stringer.

The number of cycles to failure (see Table 1) consisted of the average value of the last observation of the undamaged panel and the failure relief (visible crack). In spite of the fact that the inspection times were chosen to avoid uncertainty regarding values of less than 5% of the failure cycles, during this period, the crack generally nucleated and propagated very fast. Hence, the final results were that the crack often propagated for whole T-cleat sections. Based on the fast propagation of the crack inside the T-cleat, the fatigue-tolerance requirements [1] investigated in this paper were only limited to a safe-life approach. No further investigations to check the structure's ability to tolerate the effect of the damage (flaw tolerance) were carried out on the damaged structure.

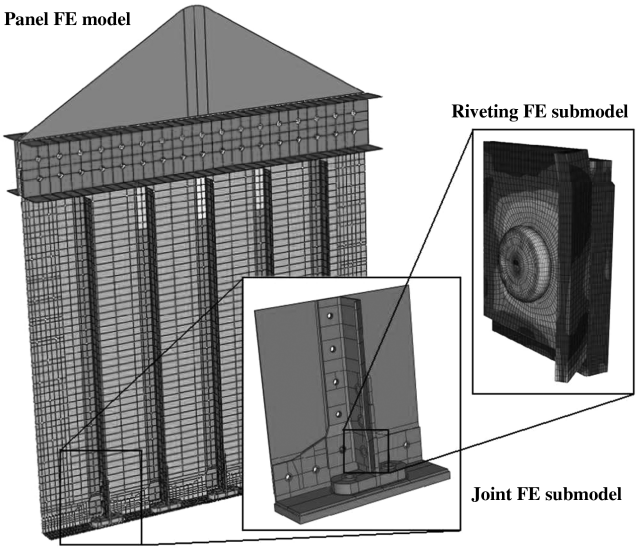

Fig. 2 FE models.

IV. Numerical FE analysis

Bearing in mind the objectives of this paper, i.e., investigating the fatigue behavior of a riveted joint, a detailed numerical analysis is fundamental to accurately estimate the stress field and to correlate a stress parameter with the fatigue life of the material. The numerical analyses were carried out using three different finite element models. The first model was a global model of the panel in which all the components were correctly modeled. To ensure accurate stress distribution around the rivets, the second model faithfully reproduced the

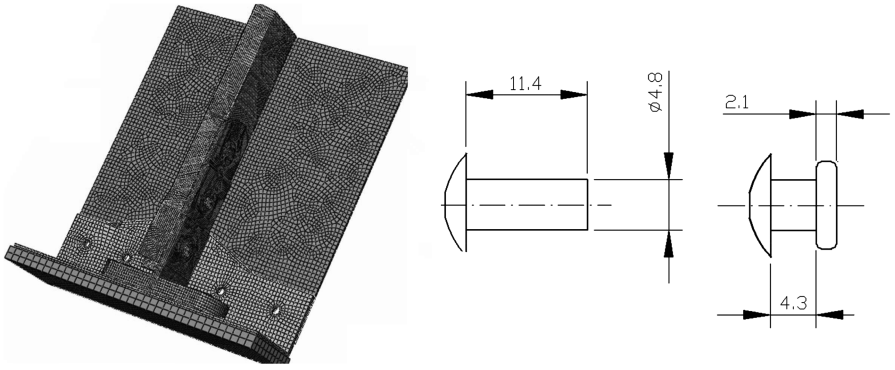

a) b)

Fig. 3 Illustrations of a) FE joint submodel and b) rivet geometry before and after plastic deformation; units are in millimeters.

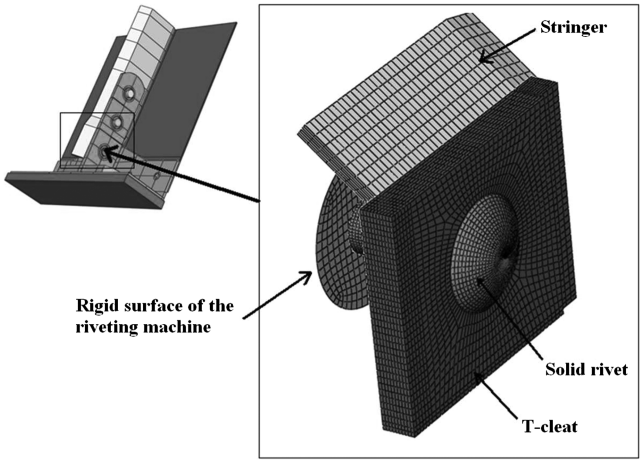

Fig. 4 Geometry used in the rivet-forming submodel.

panel joint. The third model numerically simulated the complete riveting manufacturing process. All of these models are shown in Fig. 2.

This progressive approach, based on simulation, was fundamental and allowed us to obtain the actual residual stress distributions in the riveted zone. All the models were developed using Abaqus® version 6.7, a commercial finite element software. The analysis sequence was divided into different steps. First, in order to acquire the stress field for the entire panel, the global panel model was dedicated, with particular attention being placed on the evaluation of the load distribution along the skin and the stringers. Second, starting from the global results, the joint submodel allowed us to obtain a detailed stress–strain field in the T-cleat, which proved to be useful in order to correctly describe the stress path from the stringers to the T-cleats. Finally, to also assess the residual stress field in the riveted zone, the last submodel was used to numerically reproduce the riveting process. According to the submodeling technique, the results of the global model (in terms of nodal displacements) are the boundary conditions for the joint submodel; consequently, this model reproduces the joint in detail, including the stress field (inside). The same downstream approach connects the joint submodel with the riveted submodel This approach allows an efficient balance between results accuracy and complexity/time of the analyses.

A. Panel FE Global Model

The global finite element model included all the parts of the specimen panel. The use of shell elements was suitable, due to the thin thickness of the skin, the reinforcements, and the stringers. This solution also enabled us to cut down on the computational cost of the model. The stringers were joined to the sheet by means of blind rivets, modeled as hollow beams and linked to the holes. A contact interaction (frictionless) was set up between the surfaces in contact with the stringer and the panel. The T-cleats were reproduced as a solid part; in the next submodel, this solution enabled us to obtain the exact stress distribution along the thickness. The metal sheets were made of aluminum alloy Al 2024 [22], and the T-cleat and stringers were made of aluminum alloy Al 8090-T81 [23].

B. Joint FE Submodel

As previously mentioned, the T-cleats were modeled using solid elements. Despite the fact that the T-cleat has a thin thickness and may thus be modeled with shell elements, the stress along the thickness can be important for fatigue evaluation.

Thus, a complete 3-D detailed geometry of the T-cleats was taken into account in this submodel. The T-cleat, the stringer, and the skin in the most stressed joint zone were modeled using 3-D solid finite elements (C3-D8R). The complete submodel (Fig. 3a) required about 65,000 finite elements. The interactions between the components were modeled by means of hard contacts with a friction coefficient equal to 0.3. The solid rivets were modeled as solid components and a contact interaction was introduced into the hole boundary.

C. Riveting FE Submodel

To obtain numerical residual stresses in a riveted joint it was necessary to simulate the entire riveting process. The T-cleat was connected to the stringer by means of solid rivets (MIL-STD 20470 [24]); the geometrical dimensions of the rivets are shown in Fig. 3b. Following the deformation process, the geometry of the rivet heads (diameter and thickness) served as a parameter to identify the quality of the riveting process. This geometry, together with the shank geometry and its interaction with the hole, influences the residual stress field in the structure and, consequently, the fatigue life of the joint.

To accurately simulate the riveting process used on the test panels, the dimensions of the deformed rivet heads were measured on the panel and then reproduced numerically (Fig. 4) by varying the motion law of the rigid surface, which represents the hammer of the riveting machine. The geometry considered in this submodel is related to the zone in which the failure occurs (i.e., the rivet near the constraint) (Fig. 4). The stringer, the rivet, and the T-cleat were modeled using solid elements, thus allowing us to estimate the stress variation along the thickness.

During the riveting process, the rivets are placed under high-strain deformation; for this reason, a dynamic explicit simulation is required in order to obtain a reliable solution that is representative of the real behavior. Hence, the submodel was developed using Abaqus/Explicit version 6.7 finite element software. The T-cleat consisted of 20,480 finite elements; 10,056 solid elements were used for the stringer and 7784 were used for the rivets. Because of high deformation, a general contact formulation was used to assess the contact between the parts. A friction coefficient equal to 0.3 was used between the aluminum components. The riveting process was simulated using a rigid surface (Fig. 4), which compressed the rivet head until it reached the rivet dimensions measured on the panel under unloaded conditions. The high deformation of the rivet required the use of an adaptive meshing algorithm. In Abaqus/Explicit, excessive mesh distortion was avoided by using an arbitrary Lagrangian–Eulerian [25] domain on the rivets. The rivet made of Al 2024 was modeled with an elastic plastic with linear hardening behavior (from yield point to failure condition). The stringer and the T-cleat were both modeled in a similar way, considering the application of a Al 8090-T81 material. Table 2 shows the characteristics of the materials employed in the FE software.

D. Finite Element Model Validation

Validation of the finite element model was only verified on the global model. The global model is particularly important, because all submodel boundary conditions depend on its results. Moreover, during the experimental tests, strain gauges were positioned in different zones on the panels so that it was thus possible to compare the experimental strain values with the numerical results. The complete instrumentation used consisted of 28 strain gauges

Table 2 Material characteristics for FE analysis

Material	Modulus of elasticity E, MPa	Poisson's ratio ν	0.2% yield strength σ_Y, MPa	Ultimate tensile strength σ_{UTS}, MPa	Elongation in 50 mm (2 in.) ε_f, m/m
Al 2024 [22]	73,100	0.33	317	330	0.09
Al 8090-T81[23]	77,000	0.30	324	450	0.12

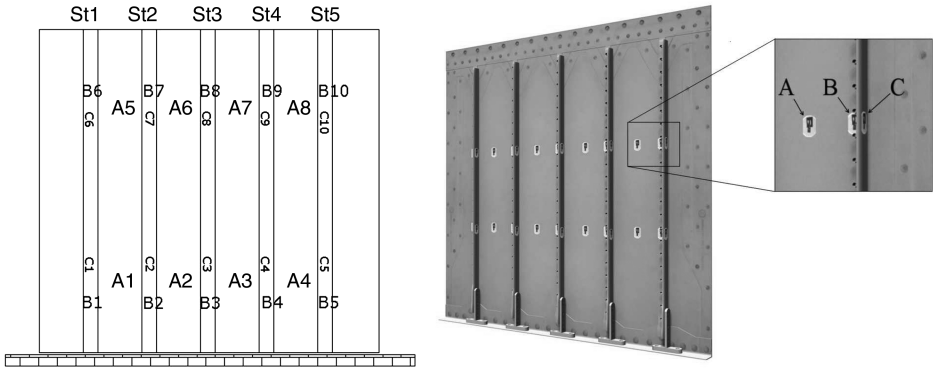

Fig. 5 Panel tested and strain-gauge position (left) and layout of the strain gauges (A, B, C) (right).

positioned in two groups at approximately one-third and two-thirds of the panel height (Fig. 5). Two strain gauges were placed at the same height on each stringer: strain gauge C was placed in the central zone of the stringer, perpendicular to the skin, and strain gauge B was placed in the central zone of the stringer parallel to the skin, with one pair per stringer group. The direction of the strain gauge was parallel to the stringer axis. Strain gauges (four per group) were placed on the skin in each bay between two stringers. These were termed gauges A and, in terms of direction, were parallel to the stringer axis. Identification of the stringer for the strain gauges and for failure identification, together with the layout of the strain gauges, is shown in Fig. 5. Only *P*2 has a complete instrumentation; *P*3 and other three panels (belonging to the same test campaign) have a reduced strain-gauge survey. The other three panels are not considered in this paper, due to the heavy computational effort needed for each simulation. The experimental strain-gauge values reported in Table 3 are therefore average values (where possible) or refer only to the *P*3 specimen. Thus, Table 3 shows a comparison between the strain measured and the FE values at a load of 19.6 kN.

From the comparison, it is possible to see that the FE values often tend to overlap on the mean (where available) values, showing that the FE models describe with a sufficiently good agreement the state of strain and stress inside the panels. The differences found are probably due to geometrical tolerances consequent to the manufacture of the specimens. Almost all the panels (representative of the real technological process) showed a more-or-less pronounced nonregular shape with a barely visible twisting and or bending of the skin plane. Considering the high variance of the irregular shapes observed, these have not been included in the FE models, which are referred to as the nominal straight configuration. Analogous behavior has been noticed by the authors in similar construction panels used for crack propagation assessment [26,27]. However, the previous work shows that a nominal numerical model is able to correctly reproduce the main structural phenomena.

Therefore, considering the previous considerations, the experimental strains are in good agreement with the corresponding FE values, especially for strain gauges C1, C6, A1, A5, B1, and B6, which were placed near the maximum-stressed T-cleat zone. In view of the fact that the absolute average error is not more than 16%, thereby also allowing for errors regarding geometrical construction and load application, the global FE model may be considered to be sufficiently accurate and reliable.

Table 3 Experimental and FE strain values at 19.6 kN

Strain gauge	Strain values, μm Experimental	FE	Relative error %	Absolute average error %
C1	468	535	12.7	16.0
C2	508	525	3.2	——
C3	461	526	12.3	——
C4	411	526	21.9	——
C5	367	524	30.0	——
C6	281	322	12.5	11.2
C7	337	319	−5.6	——
C8	298	323	7.8	——
C9	281	320	12.2	——
C10	252	307	17.9	——
A1	253	221	−14.3	14.1
A2	287	242	−18.5	——
A3	288	244	−17.8	——
A4	237	224	−5.7	——
A5	325	312	−4.0	6.6
A6	351	338	−3.9	——
A7	342	340	−0.6	——
A8	259	315	17.8	——
B1	247	286	13.5	5.3
B2	325	319	−2.0	——
B3	334	328	−1.7	——
B4	326	322	−1.4	——
B5	273	296	7.7	——
B6	269	307	12.4	10.1
B7	345	354	2.6	——
B8	340	367	7.4	——
B9	324	359	9.6	——
B10	255	313	18.6	——
			Total error %	10.6

E. Finite Element Results

Because of the fact that the panel specimens were not exactly symmetrical to a hypothetical vertical axis (the L-shaped stringers were all placed in the same direction), the results of the global FE model indicated that the most stressed joint in the panel was the first on the bottom left-hand corner. Stress distribution in the joint without the residual stress due to the riveting process is shown in Fig. 6.

Figure 6 also shows some examples of riveting forming in a section plane. In these pictures, the high plastic deformation to which the rivet head is subjected is clearly visible.

As previously explained, the numerical analysis simulated the process in such a way that the dimensions of the rivet head are exactly the same as the rivet found in the specimen panel. The riveting process induced high deformation on the rivet head and a residual stress–strain field in all the components of this submodel. The maximum circumferential stress in the T-cleat component was positioned at about one-third of the thickness from the external surface. In this section (Fig. 7), along the circumference of the hole, there were two points that clearly showed stress concentration. These two points were placed at the very beginning of the crack path observed during the experimental test (see path 1 and path 2 in Fig. 7). The absolute maximum circumferential stress occurred at the beginning of path 1 and corresponded exactly to the physical point at which the crack started. The secondary maximum circumferential stress point corresponds to the point at which a second crack nucleated and propagated until complete T-cleat failure. These results are clearly further evidence of the accuracy of the model.

The first graph in Fig. 8 shows the circumferential stress trend along the hole circumference. The two curves indicate the circumferential stress around the hole in the most stressed section (as previously illustrated); they correspond to the application of the full riveting process, to the maximum load applied on the panel

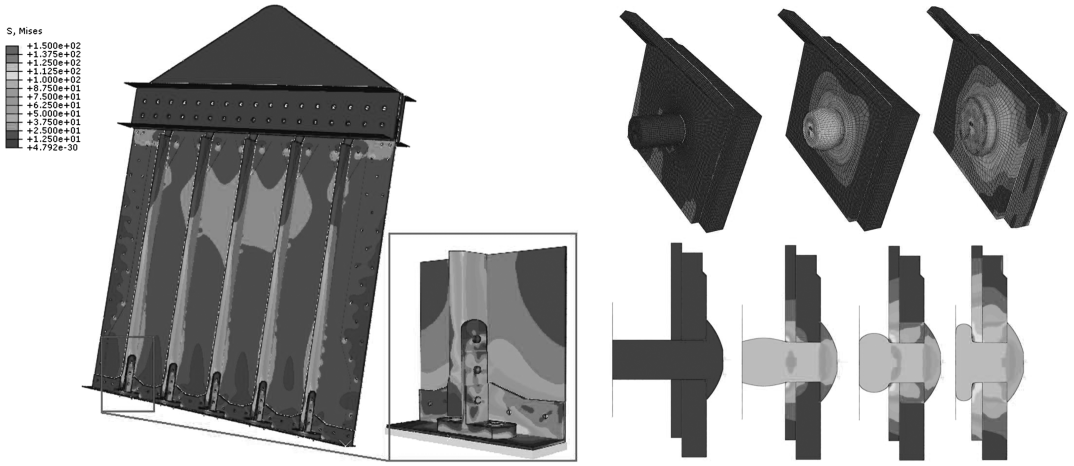

Fig. 6 Stress results of the panel, joint, and riveting FE model.

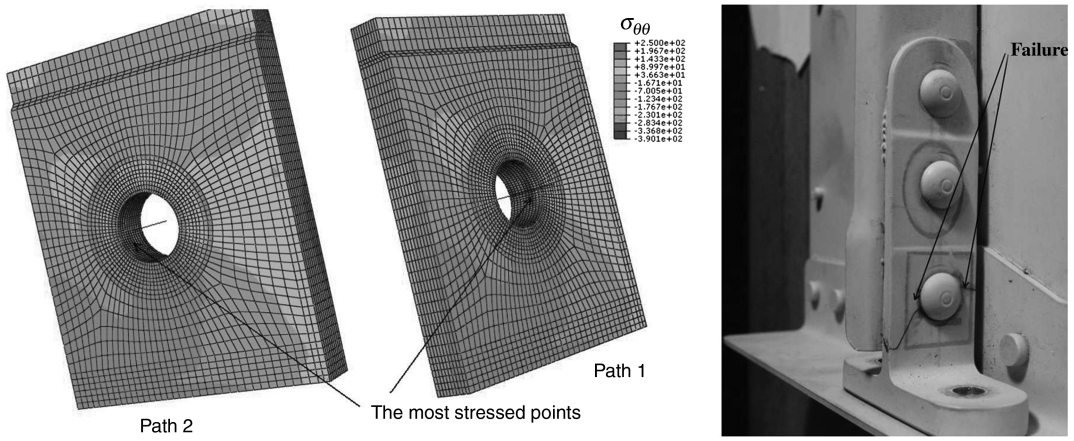

Fig. 7 The most stressed points on the riveted T-cleat (left) and experimental failure points (right). The crack on the left of the rivet is path 2 (220°); the crack at the right is path 1 (0°).

($P_{\max} = 21.6$ kN, solid line), and to the unloaded condition (dashed line). As mentioned above, the maximum circumferential stressed points are positioned exactly at 0° (path 1 starting point) and 220° (path 2 starting point) of the reference system in Fig. 7. The remaining graphs in Fig. 8 show the different stress curves, obtained from FE analyses, along path 1 of Fig. 7, starting from the maximum circumferential stress.

Numerically predicting the residual stress field is quite complex and depends on many physical parameters such as interference fit, plastic behavior, clamping force, friction coefficient, and sheet thickness. A modification of one of these parameters can lead to different residual stress values; for this reason, it is particularly important to have a detailed numerical model that considers all the existing variables. The trend of the radial and circumferential stresses are in agreement with [28] in literature; the numerical values obviously depend on all the parameters outlined previously, thus making a parametric approach quite complex. When the rivet head is squeezed, the rivet shank is placed under a compressive force that tends to enlarge the rivet hole (Fig. 9a). Generally speaking, this effect induces a plastic deformation in the rivet hole, meaning that when the squeezing force is released, the residual circumferential stresses are compressive (an advantage insofar as fatigue life is concerned). If this effect is not high enough to induce a yield condition in the rivet hole, the residual stress field is negligible. In this case, at the rivet/hole interface, there is a stress field induced by the deformed rivet that tends to enlarge the hole and to generate tensile circumferential stresses.

Because of the fact that the joint analyzed has a tensile residual circumferential stress in the most stressed point, fatigue life could be decreased. This behavior is a consequence of a failure to achieve the yield condition during the riveting process in the T-cleat (see Fig. 9b, which shows the yield zone after the riveting operation). Figure 9b clearly shows that the plastic field only affects the zone near the rivet hole on the stringer. The values of the principal stresses at the most stressed point at different loading conditions are shown in Table 4. The behavior of the principal maximum stress at the rivet/hole interface is similar to the behavior of the circumferential stresses.

V. Fatigue Evaluation

The fatigue behavior of Al 8090-T81 was described in detail by McDarmaid and Peel [29] and in [23]. Equation (1) represents the mathematical model ($R = -1$), which is in good agreement with the reference data of Al 8090-T81 [23,29]:

$$\sigma_{F\lim R=-1}(N) = A \cdot (\log_{10}(N))^3 + B \cdot (\log_{10}(N))^2 + C \cdot \log_{10}(N) + D \tag{1}$$

The coefficients for this material are $A = -7.065$, $B = 138.64$, $C = -922.14$, and $D = 2153.6$. This expression allows us to obtain a correlation coefficient $R^2 = 0.99$. Equation (1) gives a good description of the material fatigue behavior from 5×10^5 to 10^7 failure cycles. Table 5 shows the alternate fatigue-stress limits obtained from the experimental fatigue behavior of the material compared with the alternate/mean stress observed during the numerical FE analysis in the most stressed point.

Under maximum loading conditions, the most stressed point remains in an elastic field, meaning that a fatigue-life evaluation

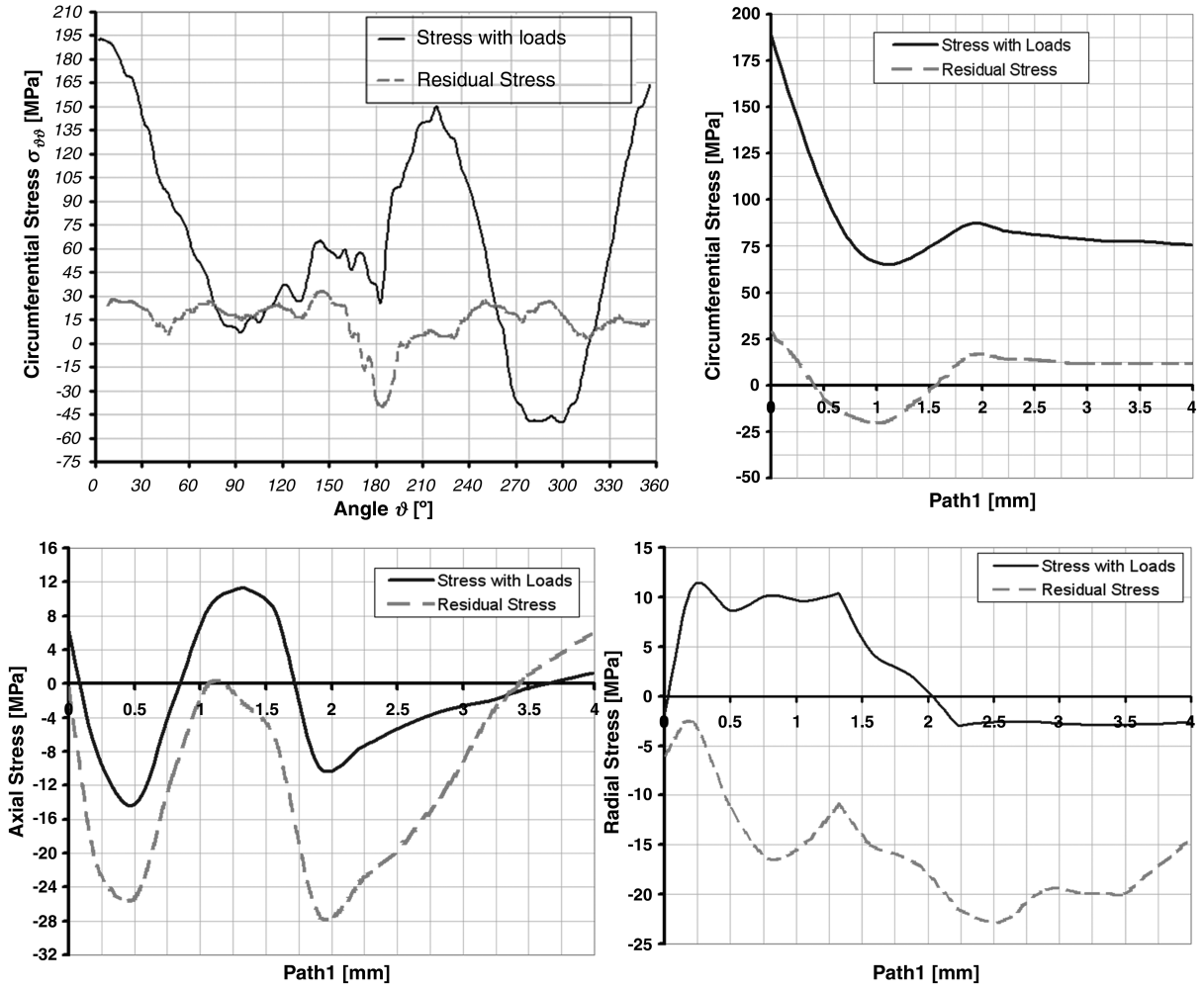

Fig. 8 Stress under loading conditions and residual stress in the most stressed hole of the T-cleat (path 1) as obtained from FE analyses.

based on stress was carried out using the maximum principal stress (near circumferential stress), since the other main stresses were able to be neglected, due to their low intensity. The mean stress effect on the alternate fatigue-stress limit was in no way negligible. Different methods can be used to consider its influence: Goodman, Gerber, Soderberg, and ASME-elliptic are just some of these methods [30]. In this paper, we used Gerber's equation (2) to consider the effect of the means stress, due to the fact that it is in good agreement with the available failure data on metals [31]:

$$\sigma_a(N) = \sigma_{\lim R=-1}(N) \cdot \left(1 - \left(\frac{\sigma_m}{S_u}\right)^2\right) \tag{2}$$

The numerical results are in excellent accord with the experimental results; Fig. 10 shows the Haigh diagrams corresponding to the failure conditions expressed in Table 5. This figure clearly shows that the failure stresses obtained from the FE analysis closely resemble Gerber's curves regarding the corresponding specimen. The effect of

Table 4 Principal stresses in the most stressed point of the T-cleat

Stress type	Residual stress, MPa	Stress, MPa: Applied load $P3$, $P_{\min} = 1.96$ kN	Applied load $P3$, $P_{\max} = 19.6$ kN	Applied load $P2$, $P_{\min} = 2.16$ kN	Applied load $P2$, $P_{\max} = 21.6$ kN
σ_{I}	29.2	45.6	192.7	47.2	209.0
σ_{II}	7.0	7.7	14.2	7.9	14.9
σ_{III}	−14.8	−14.0	−13.8	−14.0	−13.6

Table 5 Comparison with experimental and numerical values for stress to failure

Specimen	Max load, kN	Failure cycles N	Alternate fatigue-stress limit for N failure cycles $\sigma_{\lim R=-1}(N)$, MPa	Gerber alternate limit ($R = 0.1$) $\sigma_{\lim,R=0.1}(N)$, MPa	Alternate stress (FE results), MPa	Mean stress (FE results), MPa
$P2$	21.6	830,530	87.4	80.0	80.9	128.1
$P3$	19.6	1,750,630	80.9	75.5	73.5	119

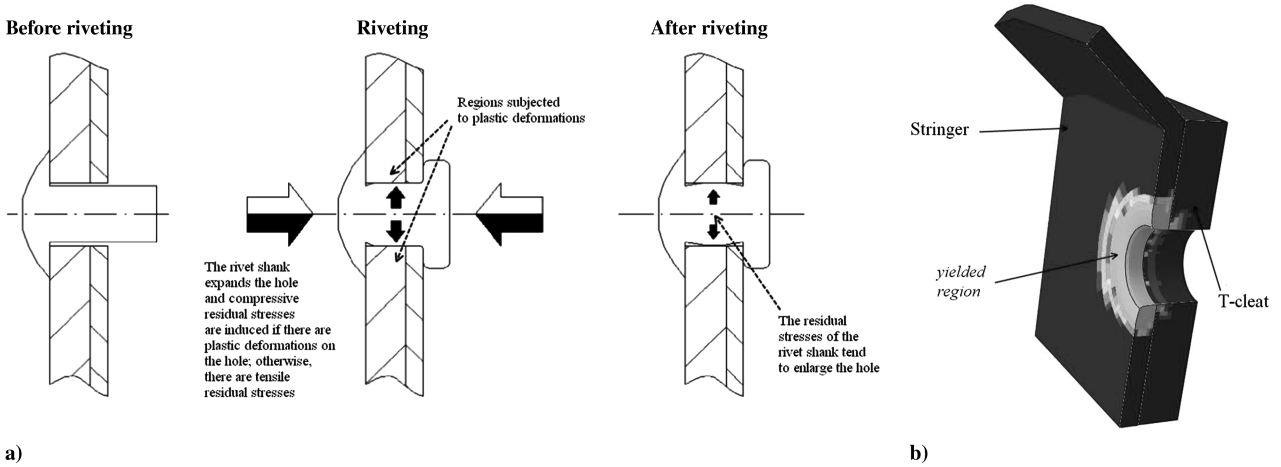

Fig. 9 Illustrations of a) stress under loading conditions and residual stress in the most stressed hole of the T-cleat (path 1) and b) yielded regions on the stringer.

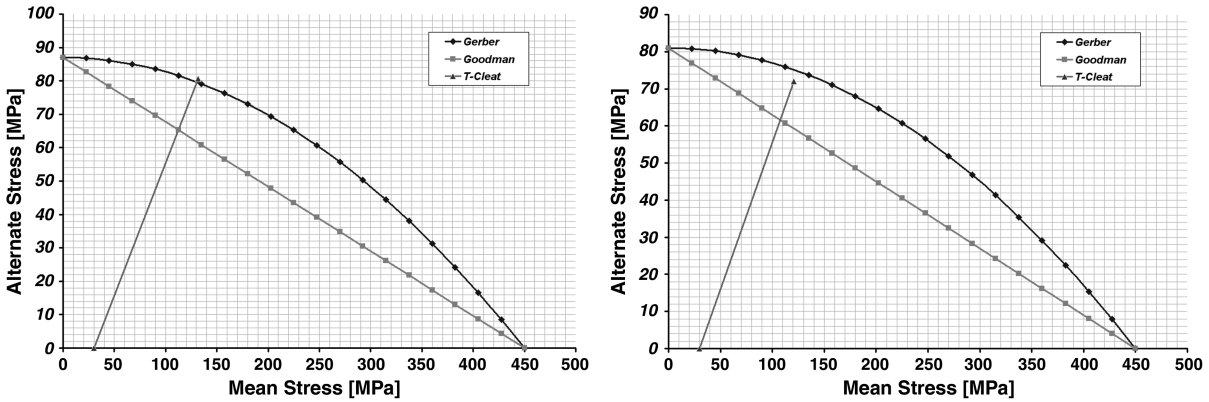

Fig. 10 Haigh diagram for specimens *P*2 (left) and *P*3 (right).

the residual stress in the most stressed point was taken into account as a shift of the mean stress value of the load paths in the Haigh diagrams.

VI. Conclusions

In this paper, the fatigue life of a riveted Al 8090 T-cleat joint, used in helicopter fuselage panels, was analyzed in detail using both experimental and numerical approaches. This analysis was performed on two specimen panels, tested using different fatigue-load ratios. The stress–strain fields of these panels were also numerically studied using three finite element models. The use of a submodeling technique in the FE approach was taken into consideration in order to investigate the stress state in the rivet area. A complex in-depth simulation of the entire riveting process was carried out in order to obtain a complete stress map that also considered the residual stresses. Since the riveting process induces high deformations of the rivet head, this simulation required an explicit FE solver, general contacts, and the arbitrary Lagrangian–Eulerian remeshing algorithm. As previously mentioned, the complete series of analyses describe an accurate stress map in the rivet zone. In particular, by observing the stress distribution on the T-cleat, it is possible to accurately localize the points at which the fatigue crack occurs. Based on the information obtained from the FE model regarding the stress fields, a fatigue analysis was conducted using the literature available on the fatigue data of Al 8090-T81. The results of this assessment are in excellent agreement with the results obtained from the full-scale component test.

References

[1] "Certification Specification for Large Rotorcraft," European Aviation Safety Agency, CS 29.571, Nov. 2008.

[2] Urban, M. R., "Analysis of the Fatigue Life of Riveted Sheet Metal Helicopter Airframe Joints," *International Journal of Fatigue*, Vol. 25, 2003, pp. 1013–1026. doi:10.1016/j.ijfatigue.2003.08.003

[3] Fung, C-P., and Smart, J., "Riveted Single Lap Joints. Part 1: A Numerical Parametric Study," *Proceedings of the Institution of Mechanical Engineers, Part G (Journal of Aerospace Engineering)*, Vol. 211, No. 1, 1997, pp. 13–27. doi:10.1243/0954410971532460

[4] Fung, C-P., and Smart, J., "Riveted Single Lap Joints. Part 2: Fatigue Life Prediction," *Proceedings of the Institution of Mechanical Engineers, Part G (Journal of Aerospace Engineering)*, Vol. 211, No. 2, 1997, pp. 123–128. doi:10.1243/0954410971532550

[5] Al-Emrani, M., and Kliger, R., "FE Analysis of Stringer-to-Floor-Beam Connections in Riveted Railway Bridges," *Journal of Constructional Steel Research*, Vol. 59, 2003, pp. 803–818. doi:10.1016/S0143-974X(02)00114-1

[6] Deng, X., and Hutchinson, J. W., "The Clamping Stress in a Cold-Driven Rivet," *International Journal of Mechanical Sciences*, Vol. 40, No. 7, 1998, pp. 683–694. doi:10.1016/S0020-7403(97)00089-1

[7] Müller, R. P. G., "An Experimental and Analytical Investigation on the Fatigue Behavior of Fuselage Riveted Lap Joints," Ph.D. Thesis, Delft Univ. of Technology, Delft, The Netherlands, 1995.

[8] de Rijck, J. J. M., Homan, J. J., Schijve, J., and Benedictus, R., "The Driven Rivet Head Dimensions as an Indication of the Fatigue Performance of Aircraft Lap Joints," *International Journal of Fatigue*, Vol. 29, 2007, pp. 2208–2218. doi:10.1016/j.ijfatigue.2006.12.010

[9] Wang, H. L., Chen, T. C., and Hsu, H. T., "Quality Verification on Riveting Process of a Pneumatic Rivet Tool," *Experimental Techniques*, Vol. 31, No. 6, 2007, pp. 57–63. doi:10.1111/j.1747-1567.2007.00184.x

[10] Deng, J. H., Yu, H. P., and Li, C. F., "Numerical and Experimental Investigation of Electromagnetic Riveting," *Materials Science and Engineering*, Vol. 499, 2009, pp. 242–247. doi:10.1016/j.msea.2008.05.049

[11] Hartmann, J., and Zieve, P., "Rivet Quality in Robotic Installation," *FASTEC '89*, Society of Manufacturing Engineers, Dearborn, MI, 1989, pp. 640–653.

[12] Matos, P. F. P., Moreira, P. M. G. P., Camanho, P. P., and Castro, P. M. S. T., "Numerical Simulation of Cold Working of Rivet Holes," *Finite Elements in Analysis and Design*, Vol. 41, 2005, pp. 989–1007. doi:10.1016/j.finel.2005.01.001

[13] Szolwinski, M. P., and Farris, T. N., "Linking Riveting Process Parameters to the Fatigue Performance of Riveted Aircraft Structures," *Journal of Aircraft*, Vol. 37, No. 1, 2000, pp. 130–137. doi:10.2514/2.2572

[14] Moreira, P. M. G. P., de Matos, P. F. P., Pinho, S. T., Pastrama, D., Camanho, P. P., and de Castro, P. M. S. T., "The Residual Stress Intensity Factors for Cold-Worked Cracked Holes: A Technical Note," *Fatigue & Fracture of Engineering Materials & Structures*, Vol. 27, No. 9, 2004, pp. 879–886. doi:10.1111/j.1460-2695.2004.00768.x

[15] Bouchard, P. O., Laurent, T., and Tollier, L., "Numerical Modelling of Self-Pierce Riveting-From Riveting Process Modelling Down to Structural Analysis," *Journal of Materials Processing Technology*, Vol. 202, 2008, pp. 290–300. doi:10.1016/j.jmatprotec.2007.08.077

[16] Porcaro, R., Hanssen, A. G., Langseth, M., and Aalberg, A., "Self-Piercing Riveting Process: An Experimental and Numerical Investigation," *Journal of Materials Processing Technology*, Vol. 171, 2006, pp. 10–20. doi:10.1016/j.jmatprotec.2005.05.048

[17] Kelly, B., and Costello, C., "FEA Modelling of Setting and Mechanical Testing of Aluminium Blind Rivets," *Journal of Materials Processing Technology*, Vol. 153–154, 2004, pp. 74–79. doi:10.1016/j.jmatprotec.2004.04.184

[18] Rans, C., and Straznicky, P. V., "Riveting Process Induced Residual Stress Around Solid Rivets in Mechanical Joints," *Journal of Aircraft*, Vol. 44, No. 1, 2007, pp. 323–329. doi:10.2514/1.23684

[19] Langrand, B., Deletombe, E., Markiewicz, E., and Drazetic, P., "Riveted Joint Modelling for Numerical Analysis of Airframe Crashworthiness," *Finite Elements in Analysis and Design*, Vol. 38, 2001, pp. 21–44. doi:10.1016/S0168-874X(01)00050-6

[20] Tate, M., "Preliminary Investigation of the Loads Carried by Individual Bolts in Bolted Joints," NACA TN1051, 1946.

[21] Rosenfeld, S. J., "Analytical and Experimental Investigation of Bolted Joints," NACA TN1458, 1947.

[22] "Metallic Materials and Elements for Aerospace Vehicle Structures," U.S. Dept. of Defense, MIL-HDBK-5J, 2003.

[23] *Properties and Selection: Nonferrous Alloys and Special-Purpose Materials*, ASM Handbook, Vol. 2, ASM International, Materials Park, OH, 2009.

[24] "Rivet, Solid Universal Head, Aluminium Alloy and Titanium Columbium Alloy," U.S. Dept. of Defense, MIL-STD-20470, 1988.

[25] *Abaqus Analysis User's Manual*, Ver. 6.7, SIMULIA, Providence, RI, 2007.

[26] Giglio, M., Manes, A., Fossati, M., Mariani, U., and Giani, C., "Comparison of Fatigue Crack Propagation Behavior of Al 2024 and Al-Li 8090 Helicopter Fuselage Panels," *Journal of Testing and Evaluation*, Vol. 38, No. 1, 2010, pp. 73–82.

[27] Giglio, M., and Manes, A., "Crack Propagation on Helicopter Panel: Experimental Test and Analysis," *Engineering Fracture Mechanics*, Vol. 75, 2008, pp. 866–879. doi:10.1016/j.engfracmech.2007.02.024

[28] Matos, P. F. P., Moreira, P. M. G. P., Pina, J. C. P., Dias, A. M., and de Castro, P. M. S. T., "Residual Stress Effect on Fatigue Striation Spacing in a Cold-Worked Rivet Hole," *Theoretical and Applied Fracture Mechanics*, Vol. 42, 2004, pp. 139–148. doi:10.1016/j.tafmec.2004.08.003

[29] McDarmaid, D. S., and Peel, C. J., "Aspect of Damage Tolerance in 8090 Sheet," *Proceedings of the Fifth International Aluminium-Lithium Conference* , Williamsburg, VA, 1989, pp. 993–1002.

[30] Zahavi, E., Torbilo, V., *Fatigue Design—Life Expectancy of Machine Parts*, CRC Press, Boca Raton, FL, 1996.

[31] *Fatigue and Fracture*, ASM Handbook, Vol. 19, ASM International, Materials Park, OH, 2009.